

Integrated Prediction of Condensation-Corrosion-Shielding Effectiveness of Metal Box with Gaps by Simulations

Jinjun Bai^{1,*}, Xiaolong Li¹, Jianshu Zhou¹, and Ming Li²

¹College of Marine Electrical Engineering, Dalian Maritime University, Dalian 116026, China

²Aviation Industry Corporation of China (AVIC), AVIC Aero Polytechnol Estab, Beijing 100028, China

ABSTRACT: With the advancement of the intelligent process, all kinds of electrical equipment are highly dense in space, and the impact of electromagnetic interference on high-precision electronic equipment cannot be ignored. Metal shielding box is one of the effective means to reduce electromagnetic interference. The heat dissipation holes on the surface of the shielded box are often used to maintain the normal operating temperature of the internal equipment, which will reduce the electromagnetic shielding effectiveness of the box. At the same time, due to the existence of capillary effect, condensation is very easy to occur at the hole gap, and the corrosion caused by it will further reduce the overall shielding effectiveness of the metal box. At present, there are few studies on the integrated prediction of “condensation-corrosion-shielding effectiveness” of metal boxes. Based on the commercial multi-physics simulation software COMSOL, this paper first simulates the condensation of a metal box in a high-humidity environment by constructing temperature, humidity, and moisture transport fields. Then, the current field and deformation field are constructed to predict the corrosion phenomenon at the gap of the metal box, and finally the electromagnetic field is constructed to predict the electromagnetic shielding efficiency of metal boxes at different frequencies. The joint multi-physics coupling simulation of condensation, corrosion, and electromagnetic shielding effectiveness phenomena is realized.

1. INTRODUCTION

With the advancement of intelligence, the storage of various electronic devices is becoming more and more intensive; the electromagnetic environment is gradually deteriorating; and the impact of electromagnetic interference on equipment cannot be ignored [1]. Metal shielded enclosure is a reliable electromagnetic protection design that ensures the proper operation of high-precision equipment [2]. At the same time, electromagnetic shielding box needs to be equipped with a ventilation hole to facilitate the heat dissipation of the internal electrical equipment. Various types of openings can seriously reduce the effectiveness of electromagnetic shielding, and there are many prediction methods for them, such as the method of moments and the finite difference in time domain method [3, 4]. With the rapid development of finite element technology, various commercial electromagnetic simulation software has been successfully applied to solve various electromagnetic compatibility problems due to its strong geometric modeling capabilities [5]. Güler used finite element technology to study the effect of hole position changes in metal boxes on the effect of electromagnetic shielding and found that different locations and sizes of holes in the electromagnetic (EM) shielding enclosure can lead to different shielding efficacy [6]. Liu et al. used finite element simulation software to study the propagation characteristics of electromagnetic waves in the crevices [7]. Ren et al. used finite element technology to propose a method for calculating the shielding effectiveness of shielding enclosures un-

der porous slit boxes [8]. Sapuan and Jenu used finite element simulation techniques to analyze the effect of the length of the penetration line on the electromagnetic efficiency of the shield enclosure [9]. At present, finite element analysis is a relatively mature technique for predicting the shielding effectiveness of shielding enclosures, and the COMSOL multi-physics simulation software used in this paper is one of the successful applications.

However, the metal shielded box that works in a humid environment for a long time is prone to condensation, and a liquid condensate film is formed on the surface. Condensation refers to the process in which the ambient humidity in the air cannot hold more water vapor when the ambient humidity in the air is greater than 1, resulting in the liquefaction of water vapor into liquid condensate. Especially in condensation-sensitive areas such as grooves, sharp corners, and ventilation holes [10], the main cause of this phenomenon is capillary condensation. From a physical and chemical point of view, the saturation vapor pressure of a gas is related to the radius of curvature of the equilibrium liquid surface, and the smaller the radius of curvature is, the lower the saturated vapor pressure is, and the lower the relative humidity is required for condensation to occur. Since the gas is in random thermal motion, the probability of hitting and staying on a concave surface is much greater than the probability of hitting a plane of the same area. Therefore, water vapor that has not yet reached saturation on the plane can preferentially condense on the concave surface. This is also the reason that the gaps between mechanical parts in the marine atmosphere, the gaps between oxide films, dust or corrosion

* Corresponding author: Jinjun Bai (baijinjun@dlmu.edu.cn).

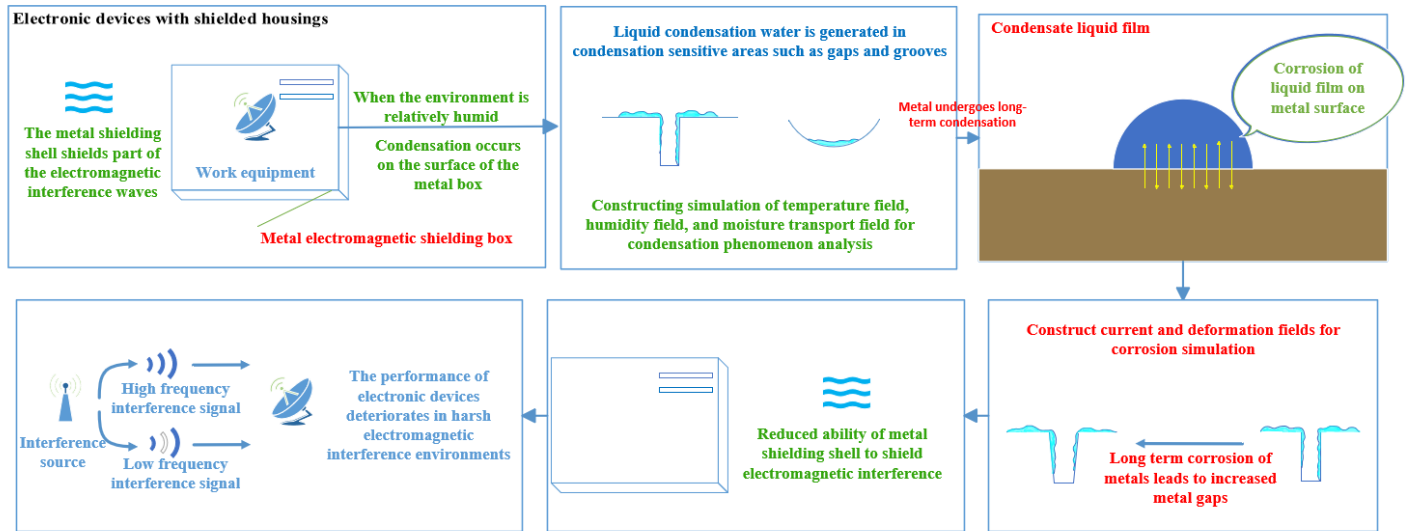


FIGURE 1. Integrated design and construction process.

products on the metal surface are easy to condense water vapor to form a liquid film [11]. Long-term erosion of liquid condensate will cause corrosion of the shielding box, in particular, in sensitive parts of condensation and corrosion, such as sharp corners of grooves such as ventilation holes. Long-term corrosion leads to deformation of the gaps [12]; the shape of the vent of the shielding box is changed; and the anti-electromagnetic interference of the metal electromagnetic shielding box is reduced, which affects the working performance of the protective equipment. Therefore, it is important to study the mechanism of this process.

At present, there are few studies on the process of condensation and corrosion leading to the change of electromagnetic shielding efficiency; therefore, this paper proposes to construct a condensation and corrosion multiphysics model using COMSOL commercial software. The results were input into the simulation study of electromagnetic shielding effectiveness to realize the integrated prediction of condensation, corrosion, and electromagnetic protection. The structure of this paper is as follows. Section 2 proposes the core construction idea of multiphysics. Section 3 constructs a multiphysics field model for condensation and obtains the distribution of condensed water in the gaps. Section 4 simulates the corrosion deformation process in the presence of condensate, obtains the deformation parameters after corrosion, and inputs them into the electromagnetic simulation model. Section 5 realizes the simulation of electromagnetic shielding efficiency and analyzes the changes of electromagnetic shielding efficiency before and after corrosion of the shielding box in detail.

2. THE CONSTRUCTION IDEA OF MULTI-PHYSICS INTEGRATED DESIGN

Figure 1 shows the overall construction idea of the integrated multiphysics design.

Firstly, based on COMSOL multiphysics field simulation software, this article constructs a multiphysics field coupling solver that includes temperature field, humidity field, and moisture transfer field, to simulate the condensation phenomenon of metal electromagnetic shielding box with air exchange holes in humid environments. Due to capillary condensation, a condensation film will form on the surface of the ventilation hole gap, and its specific location and content can be predicted.

Secondly, based on COMSOL software, construct a multiphysics field coupling solver that includes current field and deformation field. Predict the corrosion phenomenon of the ventilation holes in the metal shielding box based on the location of the liquid film on the metal surface, and quantitatively analyze the deformation of the ventilation holes after a period of corrosion.

Finally, the metal shielding boxes before and after corrosion were placed separately in the electromagnetic field for electromagnetic simulation. Through joint debugging with MATLAB software; the changes in electromagnetic shielding effectiveness of the metal shielding boxes before and after corrosion were calculated under different interference frequencies; and the mechanism of performance changes was analyzed, providing a theoretical basis for subsequent applications in electromagnetic shielding design.

3. CONDENSATION OF METAL SHIELDING BOX

The electromagnetic shielding box model used in the simulation is shown in Figure 2, and this rectangular shielding box is a typical shielding box model. The material of the shielding box is aluminum, with five fully enclosed faces, one side with two ventilation holes for internal equipment to release heat and maintain temperature balance. The thickness of the box wall is 0.5 cm, used to isolate external electromagnetic interference and protect the electromagnetic performance of internal equipment. The length and width of the metal shielding box are

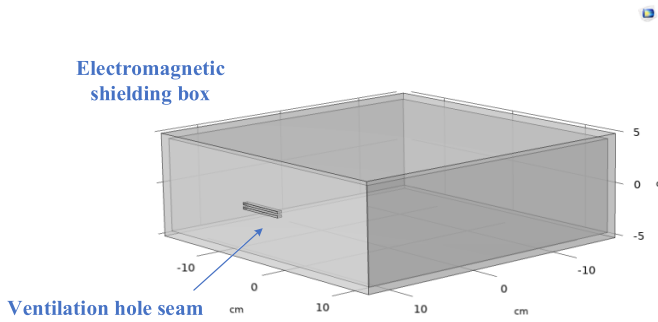


FIGURE 2. Electromagnetic shielding box model.

30 cm, and the height is 10 cm. The air exchange holes are set in two rectangular shapes with the same horizontal position and a spacing of 0.2 cm between the top and bottom. The length of the air exchange holes is 5 cm, and the width and height are 0.5 cm and 0.2 cm, respectively.

In order to simulate the condensation of the device in a humid environment, we set the model environmental conditions to simulate 24-hour temperature and humidity changes in Dalian, China. Dalian is a coastal city with high humidity, which is a typical coastal urban climate and prone to condensation. The condensation of shielding boxes was simulated in this environment.

Condensation is a physical phenomenon that involves many factors such as temperature and humidity. We simulate this complex natural phenomenon by using COMSOL commercial software to construct temperature fields, laminar flow fields, and moisture transport fields in the air. By coupling the temperature field with the laminar flow field, a non-isothermal flow coupling field is constructed. Then, the temperature field is coupled with the physical field interface of moisture transport in the air to construct a thermal wet coupling field. Finally, the laminar flow field is coupled with the interface of moisture transport in the air to construct a water flow separation dynamic coupling field. As shown in Figure 3, the simulation of condensation phenomenon is achieved through the coupling of multiple physical fields.

By constructing a condensation multiphysics field solver, the process of liquid condensation water film formation on the ventilation hole seam sidewall of an electromagnetic shielding box in a humid environment is simulated. The outer air part of the electromagnetic shielding box is set as a humid air attribute, and the wall surface at the hole seam of the electromagnetic shielding box is set as a humid surface boundary to simulate the entire process of humid air condensation on the wall surface.

The temperature field control equation adopts the temperature formula (1) and Fourier thermal conductivity law formula (2) for heat transfer control;

$$\rho C_p \frac{\partial T}{\partial t} + \rho C_p u \cdot \nabla T + \nabla \cdot q = Q + Q_{ted} \quad (1)$$

$$q = -k \nabla T \quad (2)$$

where ρ is the density, T the temperature, t the time, u the velocity field, Q the heat source, q the heat flux vector, q_0 the inward heat flux, Q_{ted} the viscous heat, k the thermal conductivity coefficient, and C_p the constant pressure and volume. In

most cases, if solid heat transfer only considers conduction, formula (1) energy law can be used to describe it. The final step is to use formula (2) Fourier's law of thermal conductivity to define the heat transfer flux vector. At this point, heat transfer flux q will be defined as proportional to the temperature gradient, namely $q = -k \nabla T$ [13].

The control equation for the laminar flow field is set to solve both the Navier-Stokes formula (3) and continuity formula (4) simultaneously.

$$\rho \frac{\partial u}{\partial t} + \rho(u \cdot \nabla)u = \nabla \cdot [-pI + K] + F \quad (3)$$

$$\frac{\partial \rho}{\partial t} + \nabla \cdot (\rho u) = 0 \quad (4)$$

where u is the fluid velocity, p the fluid pressure, ρ the fluid density, and K the viscous stress tensor. The terms in the equation correspond to inertial force $\rho \frac{\partial u}{\partial t} + \rho(u \cdot \nabla)u$, pressure and viscous force $\nabla \cdot [-pI + K]$, as well as external force F acting on the fluid. The Navier-Stokes equation represents the conservation of momentum, while the continuity equation represents the conservation of mass [14].

The content of condensed liquid water is calculated by solving the following formula (5)

$$M_v \frac{\partial c_1}{\partial t} = -g_{evap} \quad (5)$$

Among them, M_v is the molar mass of water, and g_{evap} is the evaporation flux which is derived from the saturation condition formula (6) on the surface of the shielding box wall:

$$\text{if } (c_v \geq c_{sat} \parallel c_0 > 0), \quad g_{evap} = K * (c_{sat} - c_v) * M_v \quad (6)$$

Among them, c_v represents the concentration of water vapor in the air, c_{sat} the concentration of saturated water vapor, c_0 the initial liquid water concentration on moist surfaces, and K the evaporation rate factor.

Under supersaturation conditions, $c_v \geq c_{sat}$, there is condensation on the surface, and the flux is negative (the outflow flux at the boundary of the computational domain) equal to $K * (c_{sat} - c_v) * M_v$. The concentration of liquid on the surface increases.

Due to the capillary effect, condensation is easier at the ventilation holes of the box. In order to simulate the capillary effect of condensation, the evaporation flux is modified, and the judgment condition is set to $c_v \geq 0.9 * c_{sat}$ to simulate the capillary effect during the condensation process. This allows condensation to occur before the water vapor concentration in the air fully reaches saturation.

The relative humidity change in the condensation simulation environment is shown in Figure 4. The relative humidity of the environment is greater than 1 between 3 and 7 hours in the morning, and is less than 1 at other times. Therefore, the electromagnetic shielding box undergoes condensation phenomenon between 3 and 7 hours. The concentration change of liquid water on the surface of the air exchange hole is shown in Figure 5. Condensate gradually forms between 4.5 and 6 hours, and the concentration of condensate decreases approximately between 6 and 7 hours.

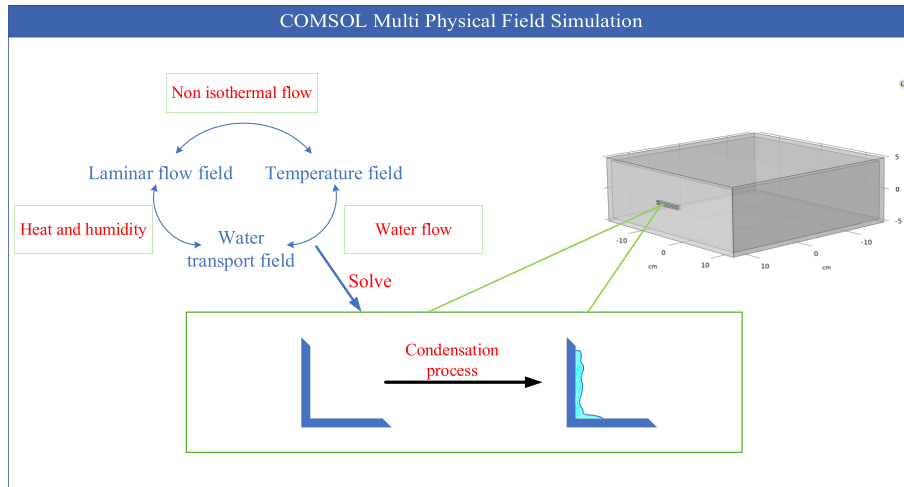


FIGURE 3. Coupling solution of multiple physical fields in the condensation process.

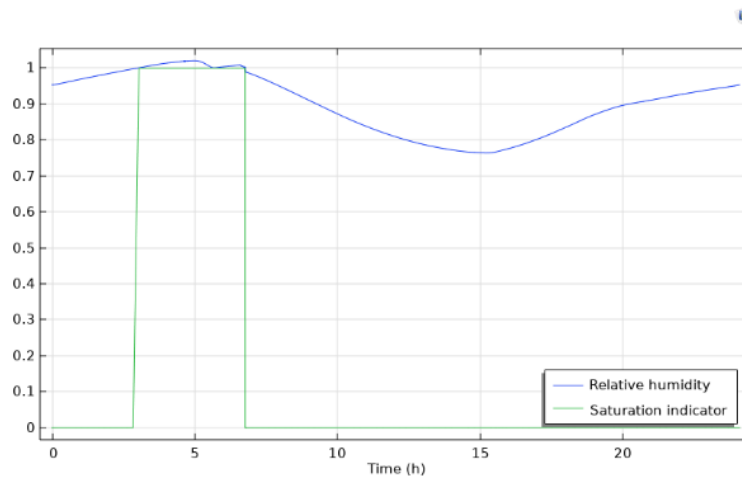


FIGURE 4. Changes in ambient relative humidity.

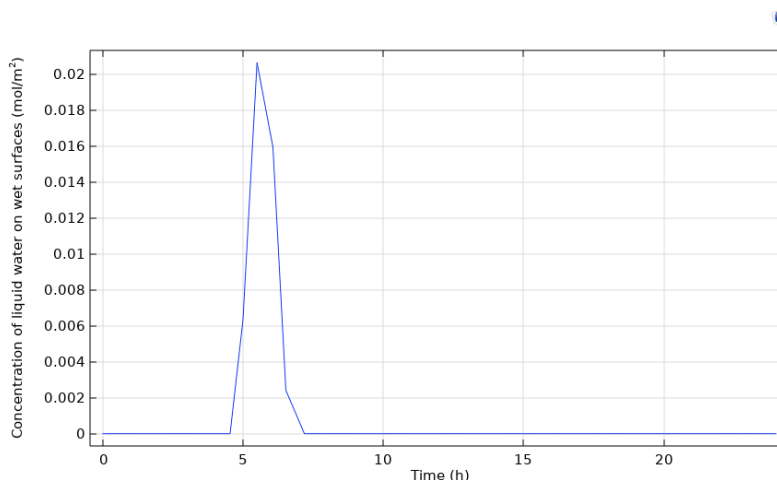


FIGURE 5. Changes in liquid water concentration on the surface of the ventilator.

With changes in environmental conditions, condensation liquid water is generated at the ventilation hole of the shielding box, and the content gradually increases during the condensation period. Moreover, due to capillary condensation, a higher

amount of condensed water is generated on the lower surface and both sides of the air exchange hole walls. The concentration of liquid water generated on the air exchange hole walls is shown in Figure 6.

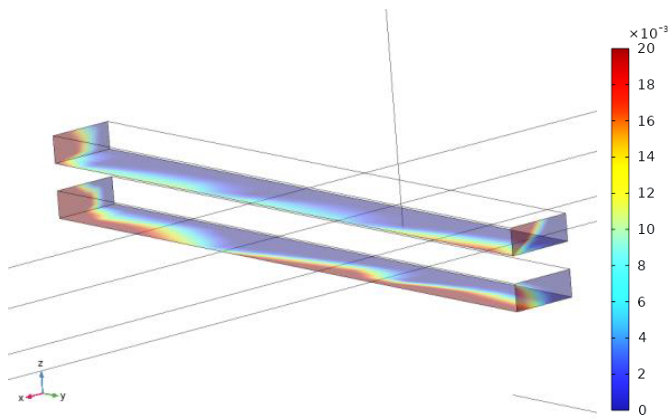


FIGURE 6. Distribution of condensate water content in square air vents.

4. CORROSION OF METAL SHIELDING BOX

For the corrosion of the metal shielding box, a solver containing current field and deformation geometric field was constructed for simulation, and a multiphysical field coupling simulation was constructed on the undeformed boundary and deformation electrode surface to simulate the corrosion phenomenon on one side of the sidewall. The schematic diagram is shown in Figure 7. The MULTifrontal Massively Parallel sparse direct Solver (MUMPS) is used in simulation for solving, and the MUMPS algorithm has high efficiency and speed in dealing with large-scale sparse linear equation systems, which can effectively improve the solving speed of corrosion simulation.

Due to the discovery in the condensation simulation that condensation is prone to occur on the side walls of the ventilation holes in the shielding box of the box, resulting in a significant amount of condensation water, the corrosion on the side walls of the ventilation holes in the shielding box is more severe. Therefore, the corrosion deformation of the side walls of the ventilation holes is simulated in the corrosion simulation. The study used a uniform thin film of liquid water attached to the sidewall surface to make the simulation effect more significant, as shown in Figure 8.

Set the blue side as the metal sidewall surface, which is the electrode surface. Due to the presence of settled salt mist in the liquid film, set Al in 4 M NaCl as the corrosive wall material to simulate electrochemical corrosion on the sidewall surface. The left side of the blue side is the direction of metal corrosion, and the gray color on the right side of the metal wall is the liquid condensate film we set, which is also the electrolyte in the corrosion simulation.

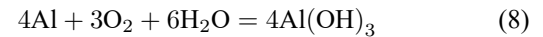
For the setting of liquid water film thickness, based on the calculated liquid film concentration value during condensation, we take 0.2 mol/m^2 as the liquid water concentration on the sidewall surface. The liquid film thickness can be calculated based on the surface liquid water concentration, and the calculation formula is shown in formula (7).

$$d = \frac{M * c}{\rho} \quad (7)$$

Among them, d represents the thickness of the liquid film, M the molar mass of water, c the concentration of water in the

film, and ρ the density of water. According to the calculation, the thickness of the liquid film is $0.36 \mu\text{m}$.

Electrochemical corrosion occurs during the corrosion process, and the aluminum box forms oxygen absorption corrosion with electrolyte solution and oxygen. The chemical equation is shown in formula (8).



Due to the long-term operation of the simulated shielding box in a humid environment, a liquid water film is set to exist and corrode the metal. The electrolyte current density vector during the corrosion process is shown in Figure 9.

After 3500 hours of corrosion, the edge of the air exchange hole in the metal shielding box gradually underwent severe deformation, as shown in Figure 10.

According to the corrosion results graph, it can be seen that after corrosion, the metal air exchange hole will undergo deformation on the inner side of the sidewall. Moreover, due to the high concentration of condensate water on the lower side of the sidewall, the corrosion degree on the lower side of the sidewall is more severe than the upper side, and the deformation is also more severe. The upper side deformation is about 3 mm, and the lower wall deformation is about 3.1 mm, which increases the length of the air exchange hole and leads to changes in the electromagnetic compatibility of the shielding box. The shape change of the air exchange hole in the box is equivalent to a hexagon, as shown in Figure 11.

5. ANALYSIS OF ELECTROMAGNETIC SHIELDING EFFECTIVENESS OF THE SHIELDING BOX

After the corrosion of the metal shielding box, the electromagnetic protection effectiveness of the metal shielding box changes. The shielding effectiveness of the metal shielding box before and after corrosion is simulated, and the influence of the corrosion phenomenon of the air exchange hole on the electromagnetic shielding effectiveness of the box is studied.

Electromagnetic shielding effectiveness simulation uses electromagnetic wave interference, with the interference source set as radiation from a biconical antenna. The simulation uses frequency domain analysis. The electromagnetic wave terminal type adopts a cable model, using a 1 V voltage source as the excitation source input. The characteristic impedance of the port is set to 50Ω , and the electromagnetic shielding effectiveness test point is located at the center of the shielding box. The electric field strength of the test point can be directly solved by electromagnetic field simulation. The distance between the electromagnetic shielding box and the biconical radiation antenna is 5 m, which is simulated in the far field, as shown in Figure 12.

Electromagnetic field simulation is achieved by constructing an electromagnetic field module using COMSOL software, and the shielding effectiveness calculation of the shielding box under different interference frequencies is achieved through joint simulation with MATLAB software, as shown in Figure 13.

Through electromagnetic field simulation, the electric field strength $E1$ of the test point without electromagnetic shielding box protection, $E2$ of the test point with electromagnetic shield-

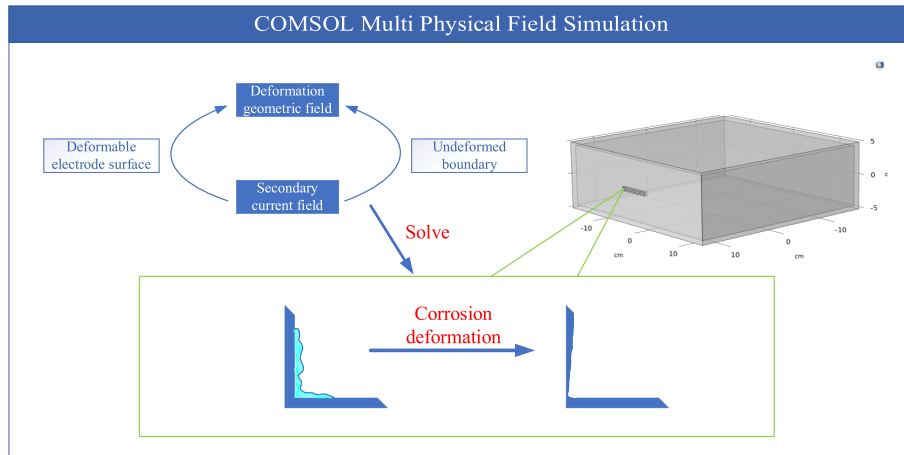


FIGURE 7. Construction of multiple physical fields for corrosion.

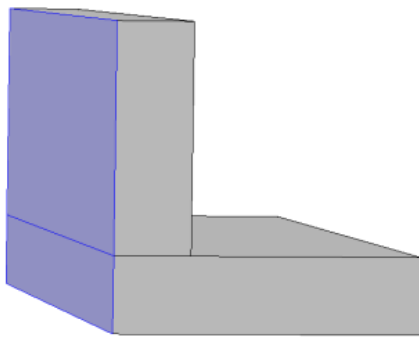


FIGURE 8. Before corrosion of the side wall of the shielding box ventilation hole.

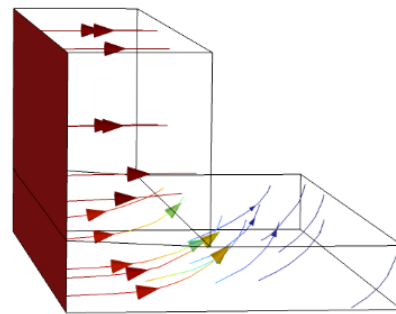


FIGURE 9. Electrolyte current density vector.

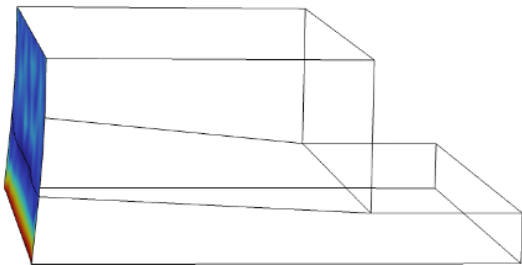


FIGURE 10. Thickness change after corrosion of the sidewall of the shielding box hole.

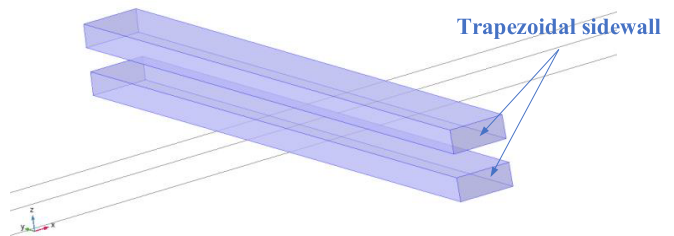


FIGURE 11. Shape of the corroded sidewall of the ventilation hole in the shielding box.

ing box protection, and E_3 of the test point with corroded electromagnetic shielding box protection were measured at a distance of 5 m from the interference source. Through joint simulation using MATLAB and COMSOL software, MATLAB software inputs different electromagnetic interference frequencies into COMSOL simulation software, and COMSOL software obtains the electric field strength of the test point after elec-

tromagnetic field simulation and then returns it to MATLAB software for calculation to obtain the electromagnetic shielding effectiveness change of the electromagnetic shielding box.

The electromagnetic interference frequency input adopts high and low frequencies separately, and the electromagnetic interference frequency input adopts from 1 MHz to 100 MHz,

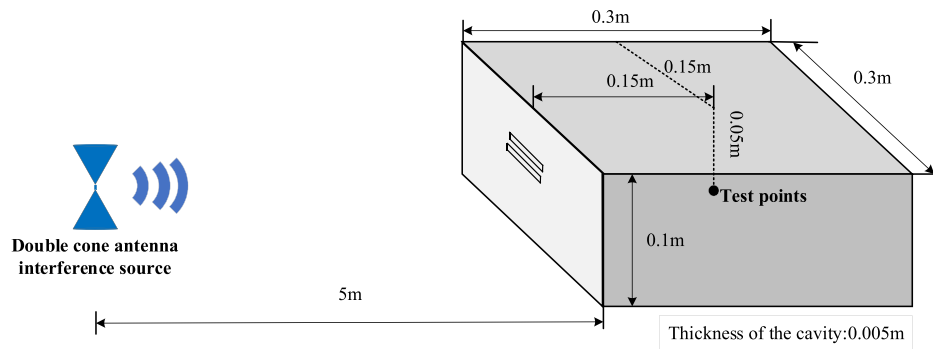


FIGURE 12. Radiation interference model of biconical antenna.

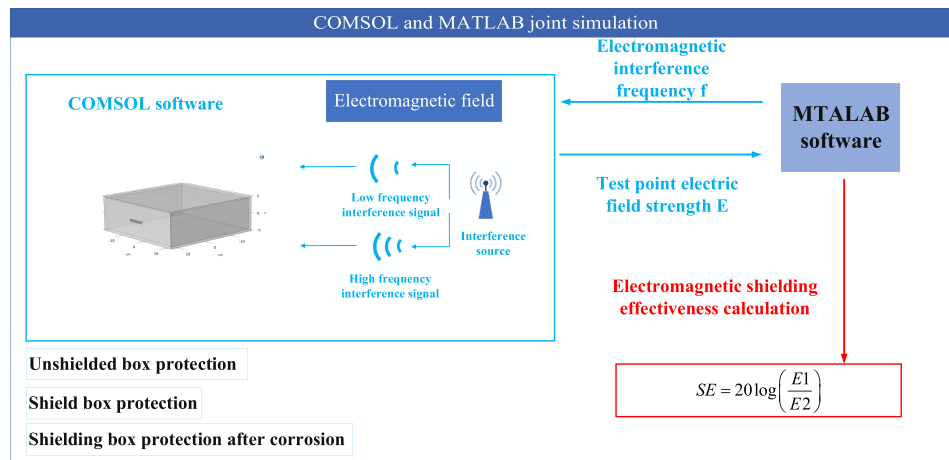


FIGURE 13. Construction of electromagnetic field simulation solver.

simulating the electromagnetic shielding effectiveness change of the metal shielding box from low frequency to high frequency. The electromagnetic shielding effectiveness of the test point is measured, and the calculation formula for electromagnetic shielding effectiveness SE_1 containing shielding boxes adopts electric field calculation, as shown in formula (10).

$$SE_1 = 20 \log \left(\frac{E_1}{E_2} \right) \quad (9)$$

The calculation formula for the electromagnetic shielding effectiveness 2 of the shielding box after corrosion is shown in formula (11).

$$SE_2 = 20 \log \left(\frac{E_1}{E_3} \right) \quad (10)$$

The changes in the shielding effectiveness of the electromagnetic shielding box before and after corrosion are shown in Figure 14. The detailed variation of electromagnetic shielding efficiency between 1 MHz and 10 MHz is shown in Figure 15(a), and the detailed variation of electromagnetic shielding efficiency of the enclosure is shown in Figure 15(b) when the interference frequency is between 40 MHz and 50 MHz.

As shown in the graph of changes in electromagnetic shielding effectiveness, with the increase of electromagnetic interference frequency, the electromagnetic shielding effectiveness

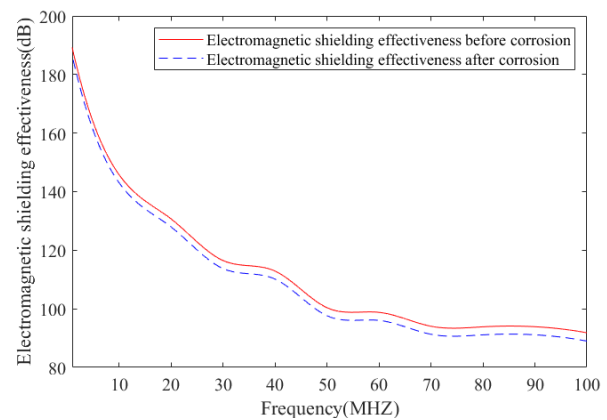


FIGURE 14. Changes in electromagnetic shielding effectiveness before and after corrosion.

of the electromagnetic shielding box before and after corrosion decreases. The reason is that the higher the interference frequency is, the easier it is to pass through the electromagnetic shielding box with holes and seams. After corrosion, the electromagnetic shielding effectiveness of the metal shielding box's air exchange holes is worse than that of the shielding box before corrosion at the same electromagnetic interference frequency, because after corrosion, the ventilation holes of the

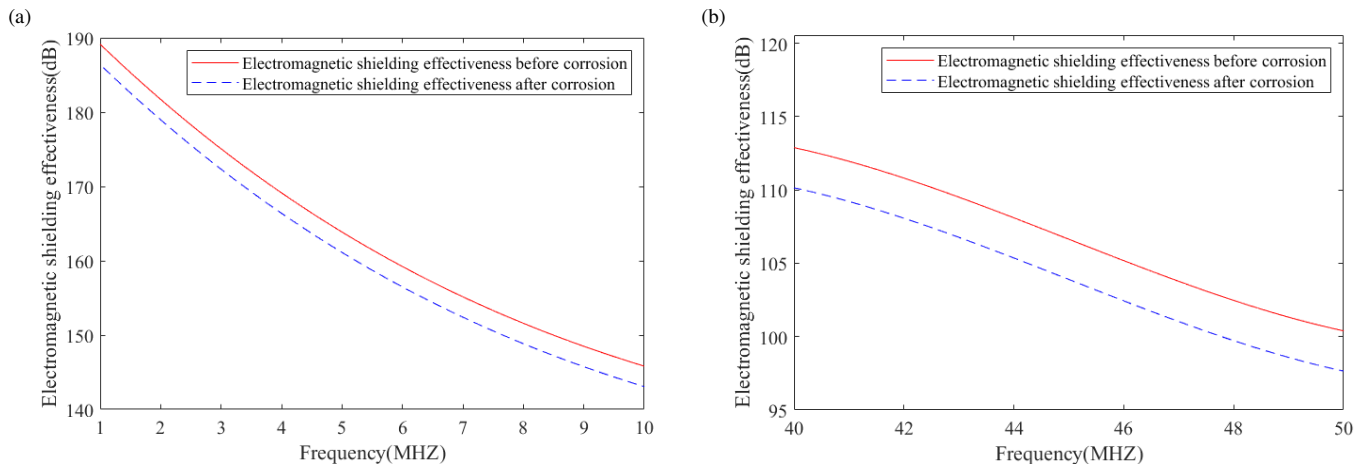


FIGURE 15. Changes in sub frequency electromagnetic shielding effectiveness. (a) 1 MHz–10 MHz, (b) 40 MHz–50 MHz.

metal shielding box become larger, resulting in a decrease in the overall shielding effectiveness of the electromagnetic shielding box. Finally, as the frequency of electromagnetic interference increases, the difference between the shielding effectiveness of the corroded electromagnetic shielding box and the electromagnetic shielding effectiveness of the box before corrosion gradually increases, because the holes and gaps in the metal shielding box become larger after corrosion, resulting in poorer shielding performance against high-frequency electromagnetic interference, and the higher the frequency of electromagnetic interference is, the more severe the deterioration effect is.

6. CONCLUSION

This article studies the condensation and distribution of condensation water in a metal shielding box in a humid environment by constructing a temperature field, laminar flow field, and moisture transfer field. It also investigates the corrosion between the liquid condensation water film and the metal after condensation, which leads to deformation of the metal and affects the electromagnetic shielding effectiveness of the metal box. By studying the changes in electromagnetic shielding effectiveness of the shielding box under different interference frequencies, it is analyzed that the decrease in electromagnetic shielding effectiveness caused by corrosion is small at low interference frequencies; however, as the electromagnetic interference frequency increases, the decrease in shielding effectiveness of the corroded box gradually accelerates, and the anti-interference ability becomes worse. The impact of corrosion on the shielding effectiveness of the electromagnetic shielding box is aggravated. This paper proposes a novel multiphysics field coupled numerical solver for the integrated design of condensation corrosion electromagnetic shielding, aiming to achieve full life prediction of electrical components in humid environments.

ACKNOWLEDGEMENT

This work is supported in part by the Youth Science Foundation Project, National Natural Science Foundation of China, under Grant 52301414.

REFERENCES

- [1] Gokce, E. C., M. D. Calisir, S. Selcuk, M. Gungor, and M. E. Acma, "Electromagnetic interference shielding using biomass-derived carbon materials," *Materials Chemistry and Physics*, Vol. 317, 129165, 2024.
- [2] Powertech Technology Inc., "Patent issued for semiconductor package with a conductive casing for heat dissipation and electromagnetic interference (EMI) shield and manufacturing method," *Electronics Newsweekly*, 2020.
- [3] Davidson, D. B., *Computational Electromagnetics for RF and Microwave Engineering*, 2nd ed., Cambridge University Press, New York, 2010.
- [4] Jiao, C., "Research on the application of finite difference time domain method for thin and thin structures in electromagnetic shielding," North China Electric Power University, Beijing, China, 2006.
- [5] Ferreira, A. and B. Auwarter, "A finite element based tool to support the understanding of electromagnetism concepts," in *2022 31st Annual Conference of the European Association for Education in Electrical and Information Engineering (EAEEIE)*, 1–5, 2022.
- [6] Güler, S., "An investigation on electromagnetic shielding effectiveness of metallic enclosure depending on aperture position," *Journal of Microwave Power and Electromagnetic Energy*, Vol. 57, No. 2, 129–145, 2023.
- [7] Liu, G., Q. Wang, L. Wang, L. Yang, Z. Yang, and A. Xu, "Research on advanced anti-interference measures in ground wave detection technology," in *2017 Chinese Automation Congress (CAC)*, 5393–5397, Jinan, China, 2017.
- [8] Ren, D., P.-A. Du, Y. He, K. Chen, J.-W. Luo, and D. G. Michelson, "A fast calculation approach for the shielding effectiveness of an enclosure with numerous small apertures," *IEEE Transactions on Electromagnetic Compatibility*, Vol. 58, No. 4, 1033–1041, 2016.
- [9] Sapuan, S. Z. and M. Z. M. Jenu, "Shielding effectiveness of a rectangular enclosure with aperture and wire penetration," in *2007 International Conference on Microwave and Millimeter Wave Technology*, Guilin, China, 2007.
- [10] Das, C., S. Halder, A. Datta, and R. Ganguly, "Influence of surface wettability on the transient characteristics of vapor condensation from humid air," *Experimental Heat Transfer*, Vol. 36, No. 7, 1034–1059, 2023.

- [11] Yang, H., K. Jayaatmaja, X. Qiu, M. Fan, M. Dejam, S. P. Tan, and H. Adidharma, "Accurate measurement of the isothermal heat of capillary condensation in nanopores using differential scanning calorimetry and adsorption/desorption experiments," *The Journal of Physical Chemistry C*, Vol. 127, No. 45, 21 980–21 988, 2023.
- [12] Jia, Z., M. Fu, X. Zhao, and Z. Cui, "Intelligent identification of metal corrosion based on Corrosion-YOLOv5s," *Displays*, Vol. 76, 102367, 2023.
- [13] Jaric, J. and Z. Golubovic, "Fourier's law of heat conduction in a nonlinear fluid," *Journal of Thermal Stresses*, Vol. 22, No. 3, 293–303, 1999.
- [14] Ju, Q. and Z. Wang, "Convergence of the relaxed compressible Navier-Stokes equations to the incompressible Navier-Stokes equations," *Applied Mathematics Letters*, Vol. 141, 108625, 2023.